



Influence of Types of Steel Poles on Measurements by Wind Speed Sensors along High-Speed Railways

J. Zhang, G. Gao, X. Xiong[†], T. Liu, F. Liu

Key Laboratory of Traffic Safety on Track of Ministry of Education, Changsha, Hunan 410075, China and School of Traffic & Transportation Engineering, Central South University, Changsha, Hunan 410075, China

[†]Corresponding Author Email: jie_csu@csu.edu.cn

(Received December 1, 2014; accepted January 12, 2015)

ABSTRACT

To find the influence of different types of steel poles on measurements by wind speed sensors along high-speed railways, the three-dimensional Reynolds-averaged Navier-Stokes equations, combined with the $k-\varepsilon$ turbulence model, were solved on an unstructured grid with a boundary layer using the finite volume method. The grid-independent validation was firstly conducted, and the accuracy of the present numerical simulation method was validated by experiments and simulations carried out by previous researchers. To ascertain angles of influence at different distances between the sensor and the virtual one, the flow field around a sensor was investigated with the method of altering the relative coordinates between the two sensors. After that, the flow fields and velocity distributions around steel poles were studied. It can be stated that behind the sensor, the closer the distance from the sensor center line, the larger the angle of influence. However, as the distance is varied from 0.3 to 1.0 m, the most adverse angles are not in excess of $\pm 20^\circ$. In addition, the steel poles have a certain influence on the measurement results of sensors. A “two-sided petal acceleration region” with a “central pistil deceleration zone” comes into being. From the perspective of regions of influence in different wind directions, the influence region of the annulus pole is basically the same. For the square and H types, when the angle is 45° , the region of effect is the largest. For the same distance between the sensor and the pole, the space required between two sensors for the single H type is larger than that required by the annulus type. Thus, it is suggested that the distance between sensors and the pole should be 1.0 m with the anemometer located on the upstream side, and the distance between two anemometers should be 0.8 m.

Keywords: High-speed railway; Grid-independence; Type of steel pole; Flow structure; Velocity distribution.

NOMENCLATURE

d	distance between the centre line of sensors and the centre of the steel pole	U	incoming flow speed
D	wind speed sensor	U_{XY}	wind speed of the point in the XY horizontal plane
h	distance between two sensors	α	wind direction relative to the railway line
L	characteristic length, which is the width of the steel pole	β	wind direction relative to the sensors
l	length of the wind speed sensor	β_e	angle of influence
R_U	velocity ratio	R_H	height ratio, which is the ratio of the height of the adverse point from the bottom of the sensor to the height of the sensor

1. INTRODUCTION

In order to prevent train accidents due to strong winds, some countries with developed railway traffic and transportation have carried out lots of research and made large effective and practical achievements (Suzuki *et al.* 2003, Diedrichs *et al.* 2007, Bociolone *et al.* 2008, Baker 2010, Liu and Zhang 2013, Rezvani and Mohebbi 2014, Hemida *et al.* 2014). All these can be summarized as three

types of measures, as follows: (1) optimization of train aerodynamic shape (Cheli 2010, Hemida and Krajnovic 2010, Zhang *et al.* 2011), (2) construction of efficient windbreak facilities (Fujii *et al.* 1999, Zhang *et al.* 2013, Zhang and Liu 2012), and (3) regulation of train operation (Fujii *et al.* 1999, Gong and Wang 2012, Liu *et al.* 2008). They greatly improve the running safety of the train under crosswinds. During this investigative process, these countries have built Strong Winds Early Warning Systems (SWEWSs) one after another

(Fujii *et al.* 1999, Gong and Wang 2012, Liu *et al.* 2008, SNCF I / SYSTRA 2004). In Japan, more than 1000 anemometers have been installed along railway lines, and regulation of operation based primarily on the wind speed has been converted into the synthetic judgement of wind speed and its direction (Fujii *et al.* 1999, Liu *et al.* 2008). In Korea, it is suggested that the distance between the wind monitoring system and the nearest obstacle should be 10 times the height of the obstacle. Therefore, the system along a high-speed railway is usually located away from the railway line, where an iron tower is set up (SNCF I / SYSTRA 2004). In France, wind speed sensors are installed on two independent dismountable masts which are 5 m high. Each one has two sensors that are 4 m above the rail level and at a distance of 4 m from the centre line of the near track (SNCF I / SYSTRA 2004). In Germany, every monitoring point has two 3-D ultrasonic anemometers which are also 4 m above the rail level and at a distance of 4 m from the centre line of the nearer track. In China, the system is mainly built along the Lanzhou–Xinjiang railway, the Qinghai–Tibet railway, and some high-speed railways that are easily affected by strong winds and monsoons (Ye *et al.* 2001, Liu *et al.* 2009, Gong and Wang 2012). At present, along the Lanzhou–Xinjiang and Qinghai–Tibet railways, the anemology stations are generally located upstream of the railway line, where the wind speed can respond to the incoming flow. However, along high-speed railways, the wind speed sensors are located 4 m above the rail level in horizontal holders which are fixed on steel poles. They are outwards and perpendicular to the line, and every monitoring point has two sensors as in some other countries. If this layout is chosen for the regulation of operation, when the wind speed sensors are in the upstream side, the measurement data will be influenced by the steel pole; when the sensors are near the pole, the effect tends to be higher; when the sensors are in the downstream side, however, due to the shielding effect of the steel pole, the sensors may be in an acceleration or deceleration zone, and thus the measurements will be unreliable and may be incorrect. In this wind environment, how to install the sensors around the pole will be particularly important. According to their research, Fujii *et al.* (1999) proposed that wind directions be judged and train operations be controlled according to wind velocities observed with windward anemometers on the bridge which connects the Kansai district with Kansai International Airport on the Kansai airport line, so in this study, the upstream layout method is also chosen for setting up wind monitoring points.

In China, according to the document "Steel Pole for Overhead Contact System of Electrified Railway (GB/T 25020-2010)", the types of steel poles along high-speed railways are always of the square, annulus, or H type, and the velocity distributions around these types of steel poles are different. If we use one method to install the sensors on poles, the measurement data may be inaccurate. Meanwhile, the detail of velocity distributions around them has not been studied deeply. Therefore, in order to find

the influence of different types of steel poles on the measurements by wind speed sensors along high-speed railways, grid-independent validation and program validation are firstly conducted to find a suitable mesh resolution and a simulation method for the follow-up research. Then the disturbance of the flow field due to the sensors themselves is studied, and the proposed distance between two anemometers is found. After that, the flow field around different types of steel poles is analysed. Finally, the velocity distributions of the poles are analysed to find a reasonable distance between them and the wind speed sensors.

2. MATHEMATICAL MODEL

According to Article 170 of the "Interim Measures for the Management of Beijing–Tianjin Intercity Railway (TG-QT106-2008)", when the wind speed reaches above 30 m/s, high-speed trains are not allowed to run into gale regions, and so the wind speed in the current paper is chosen as 30 m/s. Through the calculations, the Mach number of the resultant wind is 0.09, so the air can be considered to be incompressible. Previous publications (Bouris and Bergeles 1999; Dutta *et al.* 2008) indicate that the upstream flow is regular and the velocity distributions are almost the same under different viscous models. Therefore, taking this flow case into account, the Reynolds-averaged Navier-Stokes (RANS) equations combined with the eddy viscosity hypothesis (Fluent Inc. 2006) represent the most extensive method in engineering applications (Zhang *et al.* 2011; Asgharzadeh *et al.* 2012; Rezvani *et al.* 2013; Zhang *et al.* 2013, Wang *et al.* 2014, Zhang and Liu 2012) for computing the flow field around the steel pole. In this simulation, the SIMPLEC algorithm was used in the computational method to couple the pressure and velocity fields. The second-order upwind formulations were chosen for solving the Navier–Stokes equations. The convergence criterion was based on the residual value of the continuity equation being imposed to 10^{-7} with little fluctuation. And it was also monitored by plotting the aerodynamic force coefficients on the steel poles until they become steady with iterations.

3. COMPUTATIONAL DETAILS

In the paper, the types of steel poles chosen are the square, annulus, and H types, with cross-sections of $300\text{ mm} \times 300\text{ mm}$ ($\Phi 300\text{ mm}$), as shown in Fig. 1. Meanwhile, H types include the single-H and the double-H. Along China's high-speed railways, the types of sensors are mainly the Lambrecht hot-zone from Germany and the Vaisala ultrasonic from Finland. These two kinds of sensors are similar in their dimensions. Therefore, the Lambrecht hot-zone wind sensor is chosen for the research on the disturbance of the flow field due to the sensors themselves. Its maximal diameter D is 105 mm with a length l of 311 mm. Its exterior surface is very regular and simple, but the interior is a hole with some complex structures, so we just smooth the hole to retain its whole shape, as shown in Fig. 1 (e).

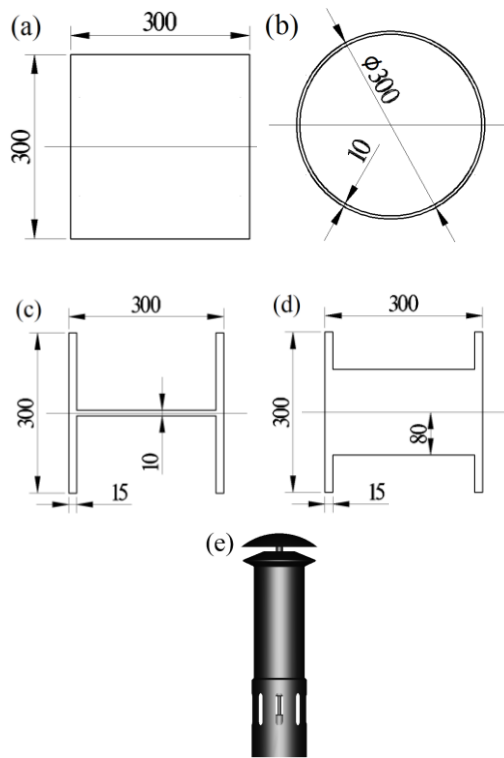


Fig. 1. Computational model (unit: mm): (a) square, (b) annulus, (c) single-H, (d) double-H, (e) hot-zone wind sensor.

In numerical simulations, the wind direction is taken into consideration, which is illustrated in Fig. 2. Then it is set as 0° , 15° , 30° , 45° , 60° , 75° , and 90° , respectively. When α is 0° , it means that the incoming flow is parallel with the railway line, and its orientation is along the positive direction of the Y axis. Meanwhile, when α is equal to 90° , it means that the incoming flow is perpendicular to the railway line. Due to the symmetry of the steel pole, as the direction varies from 90° to 180° , we can refer to velocity distributions between 0° and 90° . In addition, the distance between the two sensors is defined as h , and d is the distance of their centre line from the centre of the pole cross-section.

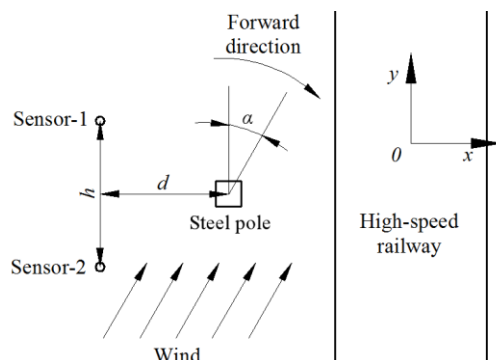


Fig. 2. Definition of the wind direction.

The steel pole along high-speed railways is an upright structure. The wind-speed sensors above the rail level are fixed on this structure at a height of 4 m. The effect of ground on the flow is much weaker at a certain height, and the computational domain

and coordinate definition are demonstrated in Fig. 3. Given the full development of the flow field, the width of the pole is chosen as the characteristic length and is denoted by L . Thus, the width and length of the computational domain are all specified as $26L$. At the same time, considering the 3-D effect of the flow field, the height is $5L$. In order to capture the flow near the wall correctly, a prism layer of 10 cells is created in a belt around the pole. The thickness of the first layer is 1.75 mm to ensure the use of the wall function in the k-epsilon turbulence model. Meanwhile, with regard to the numerical predictions, the grids that are near the surface of the pole and sensor are refined. When we investigate the disturbance of the flow field due to the sensors themselves, in the computational domain the pole will be replaced by the sensor which is located at the coordinate origin.

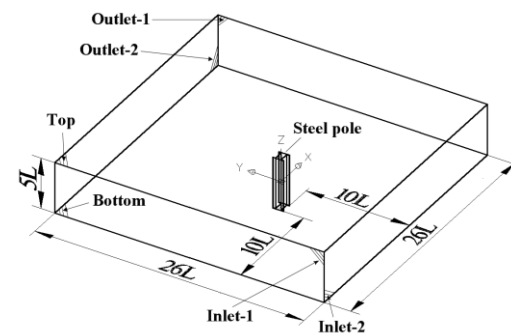


Fig. 3. Computational domain.

In Fig. 3, the surface of the pole or sensor is set as a no slip wall. Inlet-1 and Inlet-2 are treated as velocity inlets with the velocity components of the X and Y axes, respectively. The resultant velocity is 30 m/s. At the outlet, a pressure value of 0 is adopted. At the top and bottom of the computational domain, the symmetry is set.

4. RESULTS AND DISCUSSION

4.1 Grid-independent Validation and Program Validation

In order to obtain grid-independent results, numerical simulations of poles were performed on three different meshes with different numbers of cells: coarse, medium, and fine, consisting of 3.25×10^6 , 4.26×10^6 and 5.29×10^6 cells, respectively. The pole type is double-H, and the wind direction is 90° with a speed of 30 m/s. Compared with the calculated results, the velocity ratio R_U of the horizontal plane at $x = -1.0$ m is studied on three different meshes, illustrated in Fig. 4. The velocity ratio R_U is defined as follows:

$$R_U = U_{XY}/U \quad (1)$$

where U_{XY} is the wind speed of this point in the XY horizontal plane. U is the incoming flow speed.

It is discovered that the contact ratio of curves is very good. Therefore, to save computational resources, the coarse mesh is chosen for the

calculation of cases. Figure 5 shows the coarse mesh of the cross-section of the pole.

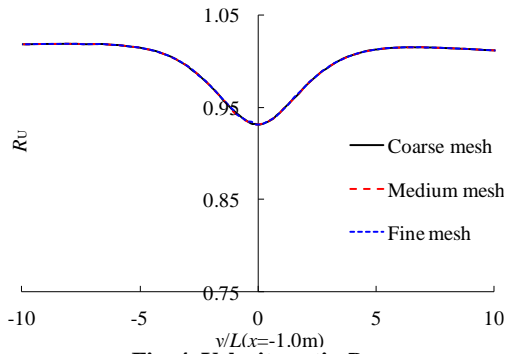


Fig. 4. Velocity ratio R_U .

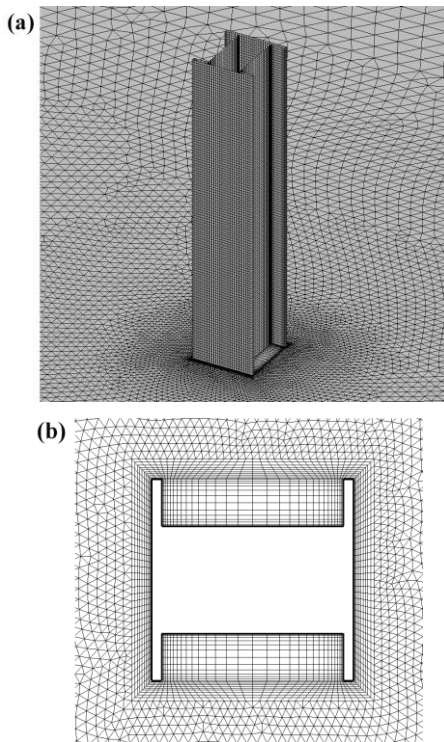


Fig. 5. Mesh distribution: (a) mesh of the steel pole and low surface, (b) mesh of the cross-section.

The next step is to validate the accuracy of the present numerical method. Figure 6 shows the validation result obtained using this program with the centre line velocity in front of the square. The experimental data are from Durao *et al.* (1988). We also found that Bouris and Bergeles (1999) carried out a numerical simulation on the flow field of a square cylinder, but it was a 2-D model and the research only investigated its vortex shedding. Based on Bouris and Bergeles' numerical simulation model, a depth with four characteristic lengths along the height direction is taken into account the 3-D effect of the flow field. Compared with the recorded values, the figure presents reasonable agreement with the experimental and simulation results.

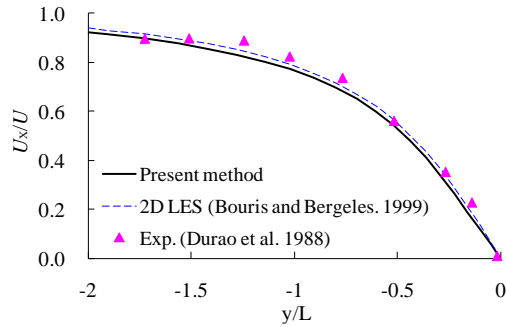


Fig. 6. Comparison with numerical and experimental results.

4.2 Flow Disturbance Due to the Sensors Themselves

In order to guarantee the accuracy of the measured data, two wind speed sensors are always installed at a monitoring point. Therefore, it is necessary to study the flow disturbance due to the sensors themselves to obtain a reasonable layout. In numerical simulations, only one sensor is located in the computational zone, while the other is a virtual sensor instead. (According to the principle of measurement by the hot-zone wind speed sensor, the data obtained are relative to their constant coefficients, convective heat transfer coefficient, passing electric current value, and so on. When these parameters are unknown, the velocity around the sensor in the simulation cannot be used to reflect the speed of the far-field airflow, so in order to eliminate the flow disturbance due to the sensors themselves, the method of setting up a virtual point and reading its speed value is chosen.)

The resultant wind velocity is 30 m/s. And the direction angle attacked is made by altering the relative coordinates between the sensor and the virtual one, as demonstrated in Fig. 7. The distance between the two sensors is defined as H and is chosen as 0.3, 0.5, 0.8, and 1.0 m. Because the sensors are symmetrical in relation to the steel pole, the angle β is only varied from 0° to 90° to achieve a comprehensive analysis of disturbance of the flow field.

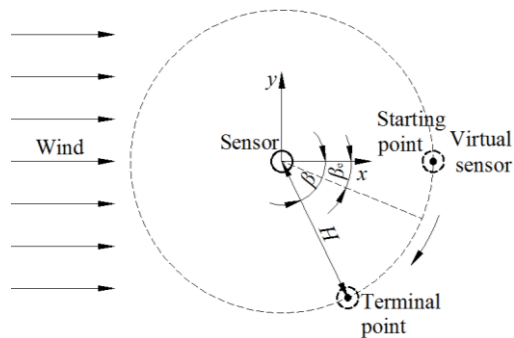


Fig. 7. Variation of the angle affected.

When angle β is 0° , it means that the virtual sensor lies at the centre line of the pole and behind it, which indicates that the measurement of the virtual sensor will be mainly affected by the pole. Because the sensor is not a regular cylinder, the velocity

ratios R_U of lines along the Z axis at distances of 0.3, 0.5, 0.8, and 1.0 m from the sensor center line, respectively, are studied to find the lowest value of R_U along the vertical height, which is the most adverse point, as shown in Fig. 8 (a).

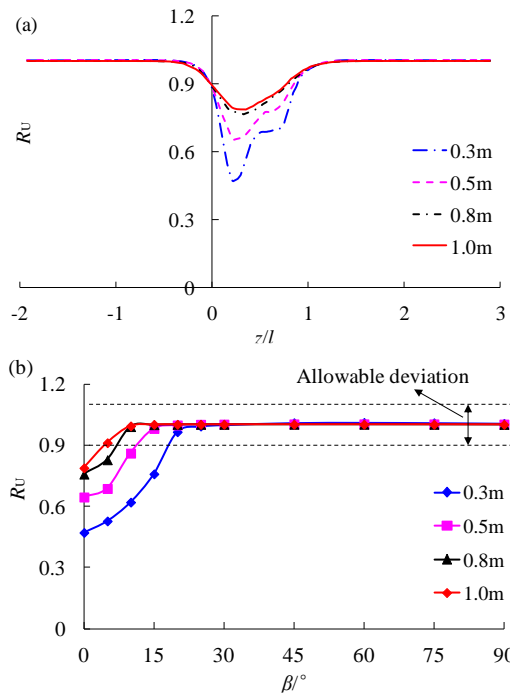


Fig. 8. Distribution of R_U : (a) R_U along the vertical height, (b) R_U under different angles.

Through detailed analysis, it is found that the height ratios R_H of the adverse points are 0.22, 0.25, 0.33, and 0.35, corresponding to the R_U values of 0.47, 0.65, 0.76, and 0.79 under these different distances. All velocity ratios are all less than 1. Here, R_H is equal to the height of the adverse point from the bottom of the sensor to the height of the sensor. Even though the allowable measured deviation of $\pm 10\%$ is taken into consideration, according to the wind measurement criterion of China's railways, R_U at adverse points do not yet reach the lowest requirements. Therefore, it is necessary to obtain the range of influence behind the wind speed sensor, named angle β_e . Figure 8 (b) shows the variations of R_U under different angles with different distances on the planes which are based on the height of the most adverse points and are parallel to the XY plane.

It is discovered that as the distance is varied from 0.3 to 1.0 m, the most adverse angles are not in excess of 20° . The closer the distance, the larger the angle of influence. Based on this investigation, the angles are obtained for different intervals as listed in Table 1. At the distance of 0.3 m, with an allowable deviation of 5%, the largest angle of impact is 19.7° . For the symmetrical location, the angle β_e is 39.4° . While at the distance of 1.0 m, it is 14.8° . If we increase the deviation to 10%, the angle decreases to 37.0° at the distance of 0.3 m and to 9.2° at the distance of 1.0 m. So an angle of $\beta \geq 20^\circ$ is suggested to avoid the disturbance of sensors

themselves and the distance $H \geq 0.8$ m.

Table 1 Angle of influence β_e

Allowable deviation	$\beta_e/^\circ$			
	$x=0.3$ m	$x=0.5$ m	$x=0.8$ m	$x=1.0$ m
$\leq 5\%$	19.7	13.7	8.8	7.4
$\leq 10\%$	18.5	11.6	7.2	4.6

4.3 Flow Fields

To understand the flow field around different steel poles, the calculated flow fields in the cross-section at $0 L$ (in the middle of the pole) along the Z axis are depicted in Fig. 9 in terms of the velocity.

Due to the effect of the blockage and the shielding influence of the steel pole, in the upstream direction, the deceleration zones occur separately in front of and behind the steel pole. The shorter the distance between the steel pole and the monitoring point, the lower the speed in that zone. However, behind the pole, the velocity at the monitoring point is much lower. As a result, a “two-sided petal acceleration region” with a “central pistil deceleration zone” comes into being, as shown in Fig. 9.

Due to an arc structure, the effect on the flow around the annulus is the same at different wind direction; therefore, the region of influence is basically the same. However, for the square and H types, due to their right-angled structures, the blockage effects can be clearly seen. When the wind direction is at 45° , the effect zone is the largest, while the smallest effect zone occurs for wind directions of 0° and 90° . In the same direction, the area of influence of the annulus is the lowest, and those of the square and H types have little difference from one another, while at 45° , the H type's area of influence is slightly larger.

4.4 Velocity Distributions

The definition of the wind direction is illustrated in Fig. 2. The model of the wind speed sensor is not located in the computational zone, but instead of a virtual point. To better ascertain the influence of the pole, on the $z = 0$ m plane, the velocity distributions of lines at distances of 0.5, 0.8, and 1.0 m, respectively, are studied. The positions of the lines are shown in Fig. 10 (a). The analysis in Section 3.2 indicates that the leeward flow field is affected more by the pole, and those of the square and H types are basically the same. Therefore, in this section, mainly the velocities at the windward flow field of the annulus and single-H types are investigated. The distribution of the velocity ratio R_U is illustrated in Figs. 10(b)–10(d) for angles of 0° , 45° , and 90° , respectively, and the range of allowable deviation of wind speed measurement in engineering applications is marked.

It is clear that the shorter the distance from the pole, the greater the impact on the monitoring point. In addition, a shorter distance from the pole causes the peak variation of velocity ratio R_U to be larger. At

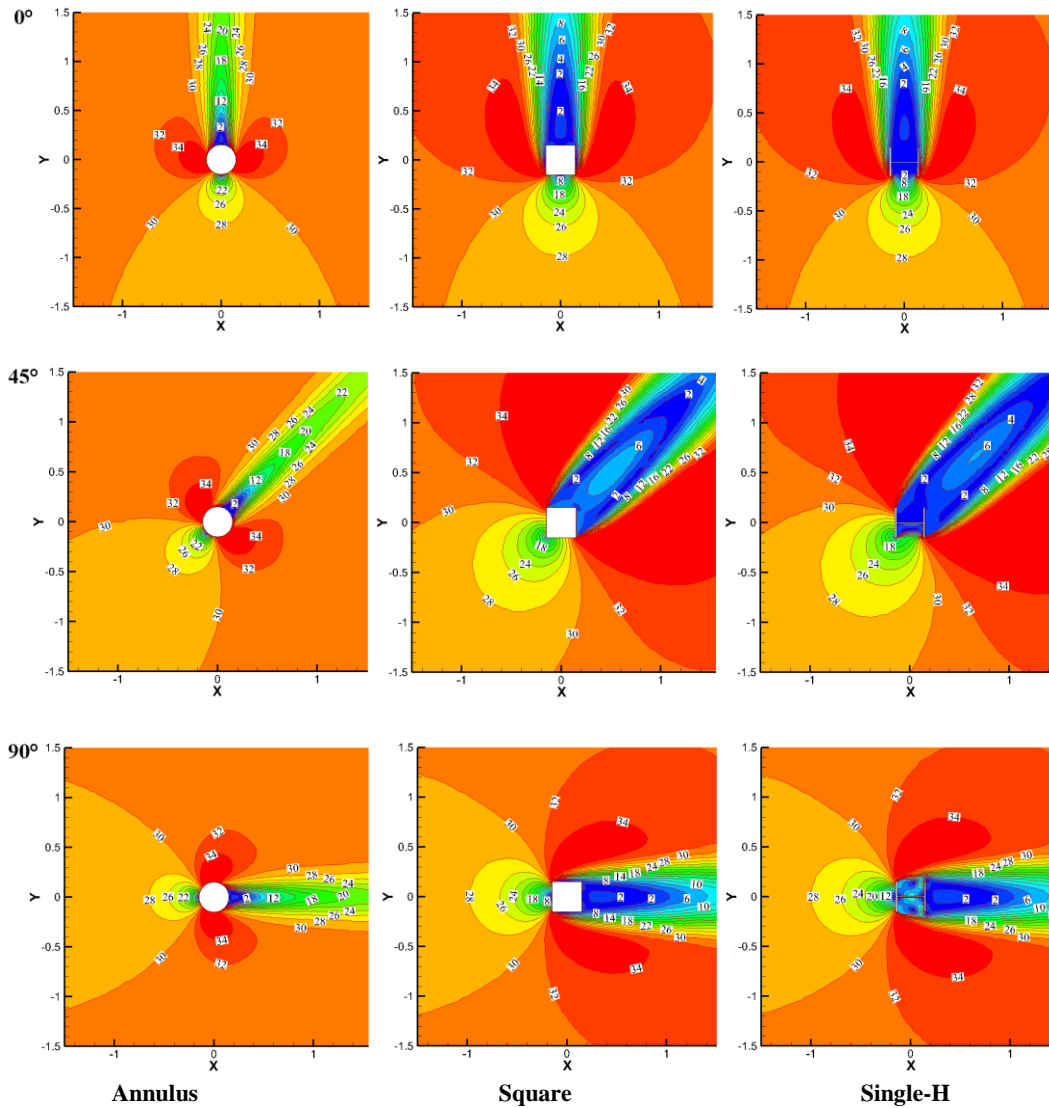


Fig. 9. Velocity contours at $z = 0$ m (unit: m/s).

the same wind direction and distance, the areas under the single-H type bounded by the curve of the velocity ratio R_U and line of $R_U = 1$ are greater than the one under the annulus type. At a direction of 0° , the region of influence is small and has a non-symmetrical distribution. At 45° , the zone is the largest and also has a non-symmetrical distribution. However, at 90° , although the area is nearly the same as that at 0° , the curve has a symmetric distribution with respect to the line at $y/L = 0$. In different directions, the values of the velocity ratio R_U along the lines range from 0.5 to 1.0 m within the allowable deviation of $\pm 10\%$ for the annulus type. For the single-H type, the situation is bad. The shorter the distance, the larger the part beyond the allowable deviation, because the possibility of receiving inaccurate data is much greater. Thus, to obtain a reasonable distance between poles and wind speed sensors, based on Figs. 10(b)–10(d), the results are listed in Table 2. (The flow fields around the square and H types are basically the same, so only that of the single-H type is analysed.)

Without considering the case of disturbance

between the sensors themselves, when the distance d of their centre line from the centre of the pole cross-section is equal to 0.5 m around the annulus type, the proper interval between two virtual sensors is $h \geq 0.32$ m. (For the symmetrical installment of the sensors, two times space is selected for the final result.) Meanwhile, when d is chosen as 0.8 and 1.0 m, respectively, as long as the virtual sensors are located on the upstream side, the measurement requirements will be met. Furthermore, for the single-H type, under the condition of $d = 0.5$ m, an interval of $h \geq 5.44$ m (2 times interval) is required to meet the requirements for all wind directions; for $d = 0.8$ m, an interval of $h \geq 4.94$ m is required, and for $d = 1.0$ m, intervals of $0.88 \text{ m} \geq h \geq 0 \text{ m}$ and $h \geq 4.48$ m are required. At the same d , the h is larger for the single-H type than for the annulus type. Therefore, the installation of the wind speed sensors on the steel pole needs to meet the requirements for the H type (there is little difference between it and the square type); that is $d = 1.0$ m on the upstream side and $0.88 \text{ m} \geq h \geq 0.32$ m. Given the flow disturbance of the flow field due

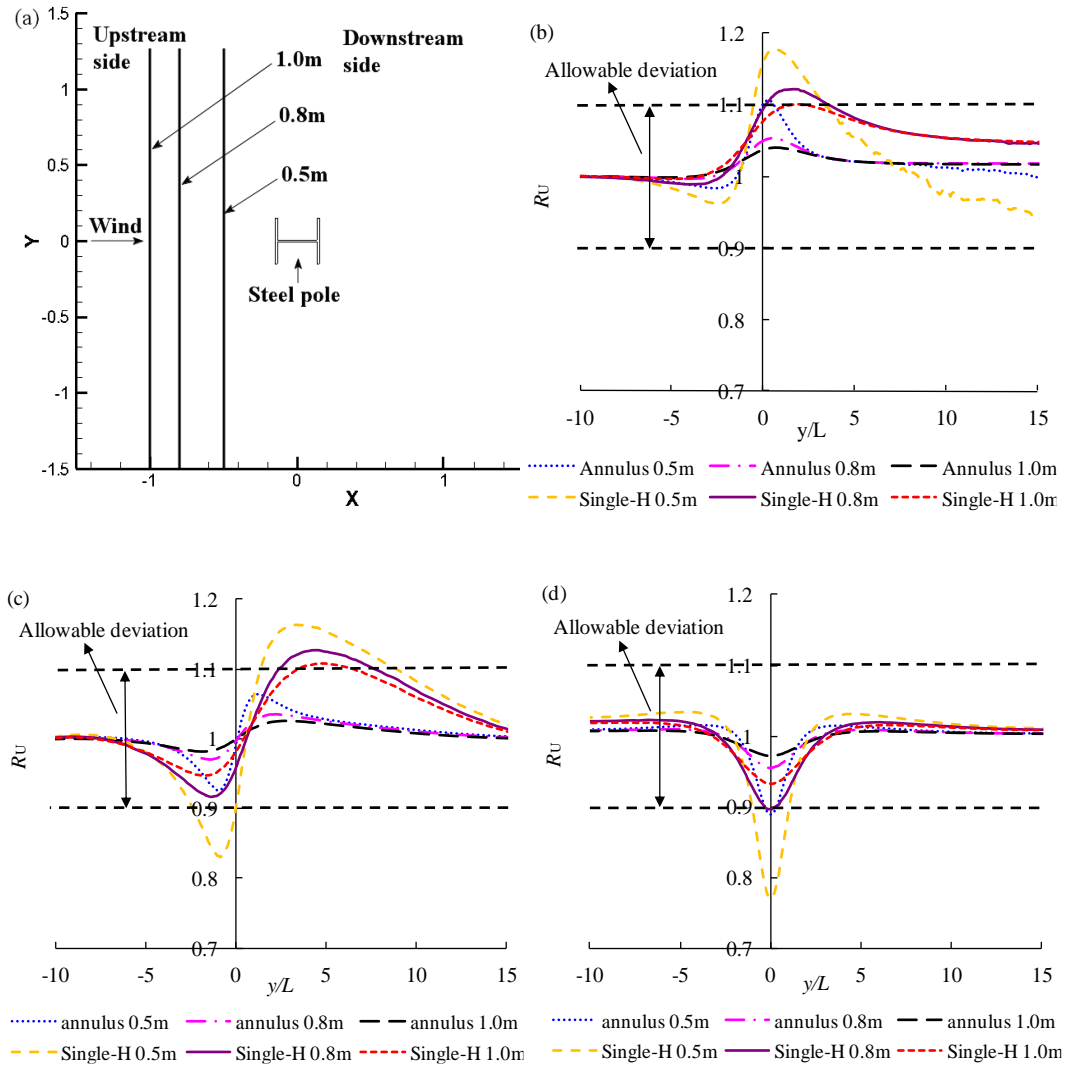


Fig. 10. Ru along the lines under different distances: (a) positions of lines, (b) wind direction at 0°, (c) wind direction at 45°, (d) wind direction at 90°.

to the sensors themselves based on the analysis in Section 3.2, it is suggested that h is 0.8 m.

5. CONCLUSION

The wind speed sensors installed along high-speed railways are always influenced by the steel pole. When the wind goes across it, due to its blockage effect, the wind speed at the sensor point will change. In this paper, RANS combined with the eddy viscosity hypothesis turbulence model has been used to investigate the velocity distribution around the sensor and different types of steel poles. The simulation method was compared with an experiment conducted by Durao (1988) and a simulation done by Bouris and Bergeles (1999), and these present reasonable agreements. Through analysis, the following conclusions could be drawn:

(1) Along the incoming flow direction, there are two deceleration zones around the steel pole. The shorter the distance, the lower the velocity around the pole, especially behind the pole. Meanwhile, a

“two-sided petal acceleration region” with a “central pistil deceleration zone” comes into being.

(2) From the perspective of the region of influence under different wind directions, the region of influence of the annulus pole is basically the same under different wind directions. For the square and H-types, when the angle is 45°, the region of effect is the largest, while the smallest effect zone occurs for wind directions of 0° and 90°. In the same direction, the area of influence of the annulus is the lowest, and those of the square and H types have little difference from one another, while at 45°, the H type’s area of influence is slightly larger.

(3) When the sensor is close to the pole, the space between two sensors tends to increase. For the same the distance d between the sensor and pole, the space h under the single H-type is larger than that of the annulus.

Thus, to install the wind speed sensors on the steel pole, it is necessary to meet the requirements of the H type, and it is suggested that the distance between

Table 2 Reasonable distance between wind speed sensors and steel poles

Steel pole	Wind direction/°	Reasonable distance between steel poles and wind speed sensors/m					
		Sensor-1			Sensor-2		
		x = -0.5 m	x = -0.8m	x = -1.0m	x = -0.5m	x = -0.8m	x = -1.0m
Annulus	0	$y \geq 0.16$	$y \geq 0$	$y \geq 0$	$y \leq -0.01$	$y \leq 0$	$y \leq 0$
	15	$y \geq 0$	$y \geq 0$	$y \geq 0$	$y \leq 0$	$y \leq 0$	$y \leq 0$
	30	$y \geq 0$	$y \geq 0$	$y \geq 0$	$y \leq 0$	$y \leq 0$	$y \leq 0$
	45	$y \geq 0$	$y \geq 0$	$y \geq 0$	$y \leq 0$	$y \leq 0$	$y \leq 0$
	60	$y \geq 0$	$y \geq 0$	$y \geq 0$	$y \leq 0$	$y \leq 0$	$y \leq 0$
	75	$y \geq 0$	$y \geq 0$	$y \geq 0$	$y \leq -0.16$	$y \leq 0$	$y \leq 0$
	90	$y \geq 0.10$	$y \geq 0$	$y \geq 0$	$y \leq -0.10$	$y \leq 0$	$y \leq 0$
Single-H	0	$y \geq 0.99$	$y \geq 1.09$	$0.44 \geq y \geq 0$ $y \geq 0.69$	$y \leq -0.16$	$y \leq 0$	$y \leq 0$
	15	$y \geq 1.69$	$0.21 \geq y \geq 0$ $y \geq 1.50$	$0.53 \geq y \geq 0$ $y \geq 1.21$	$y \leq 0$	$y \leq 0$	$y \leq 0$
	30	$0.20 \geq y \geq 0$ $y \geq 2.72$	$0.43 \geq y \geq 0$ $y \geq 2.47$	$0.63 \geq y \geq 0$ $y \geq 2.24$	$-0.29 \leq y \leq 0$ $y \leq -0.65$	$y \leq 0$	$y \leq 0$
	45	$0.41 \geq y \geq 0$ $y \geq 2.65$	$0.72 \geq y \geq 0$ $y \geq 2.30$	$1.03 \geq y \geq 0$ $y \geq 1.96$	$y \leq -0.71$	$y \leq 0$	$y \leq 0$
	60	$0.82 \geq y \geq 0.16$ $y \geq 1.56$	$y \geq 0$	$y \geq 0$	$y \leq -0.56$	$y \leq -0.32$	$y \leq 0$
	75	$y \geq 0.28$	$y \geq 0.07$	$y \geq 0$	$y \leq -0.38$	$y \leq -0.20$	$y \leq 0$
	90	$y \geq 0.31$	$y \geq 0.10$	$y \geq 0$	$y \leq -0.31$	$y \leq -0.10$	$y \leq 0$

the anemometer and the pole should be chosen as $d = 1.0$ m with the anemometer located on the upstream side, and the distance between two anemometers should be specified as $h = 0.8$ m.

ACKNOWLEDGEMENTS

This work was supported by the China Scholarship Council; the National Science Foundation of China (Grant No. U1334205); the Fok Ying Tong Education Foundation of China (Grant No. 132014); the Scholarship Award for Excellent Innovative Doctoral Student granted by Central South University of China.

REFERENCES

Asgharzadeh, H., B. Firoozabadi and H. Afshin (2012). Experimental and Numerical Simulation of the Effect of Particles on Flow Structures in Secondary Sedimentation Tanks. *Journal of Applied Fluid Mechanics* 5(2), 15-23.

Baker, C. J. (2010). The flow around high speed trains. *Journal of Wind Engineering and Industrial Aerodynamics* 98(6), 277-298.

Bocciolone, M., F. Cheli, R. Corradi, S. Muggiasca and G. Tomasini (2008). Crosswind action on rail vehicles: Wind tunnel experimental analyses. *Journal of Wind Engineering and Industrial Aerodynamics* 96(5), 584-610.

Bouris, D. and G. Bergeles (1999). 2D LES of

vortex shedding from a square cylinder. *Journal of Wind Engineering and Industrial Aerodynamics* 80, 31-46.

Cheli, F., F. Ripamonti, D. Rocchi and G. Tomasini (2010). Aerodynamic behaviour investigation of the new EMUV250 train to cross wind. *Journal of Wind Engineering and Industrial Aerodynamics* 98, 189-201.

Diedrichs, B., M. Sima, A. Orellano and H. Tengstrand (2007). Crosswind stability of a high-speed train on a high embankment. *Proceedings of the Institution of Mechanical Engineers, Part F: Journal of Rail and Rapid Transit* 221(2), 205-225.

Durao, D., M. Heitor and J. Pereira (1988). Measurements of turbulent and periodic flows around a square cross-section cylinder. *Experiment Fluids* 6, 298-304.

Dutta, S., P. K. Panigrahi and K. Muralidhar (2008). Experimental investigation of flow past a square cylinder at an angle of incidence. *Journal of Engineering Mechanics-ASCE* 134(9), 788-803.

Fluent Inc. *FLUENT User's Guide*, 2006.

Fujii, T., T. Maeda, H. Ishida, T. Imai, K. Tanemoto and M. Suzuki (1999). Wind-Induced Accidents of Train/Vehicles and Their Measures in Japan. *Quarterly Report of Railway Technical Research Institute* 40(1), 50-55.

Gong, J. and P. Wang (2012). Research on Gale Monitoring & Early Warning System of High-

- speed Railway. *High Speed Railway Technology* 3(1), 5-8, 14.
- Hemida, H., C. Baker and G. J. Gao (2014). The calculation of train slipstreams using large-eddy simulation, *Proceedings of the Institution of Mechanical Engineers, Part F: Journal of Rail and Rapid Transit* 228(1), 25-36.
- Hemida, H., and S. Krajnovic (2010). LES study of the influence of the nose shape and yaw angles on flow structures around trains. *Journal of Wind Engineering and Industrial Aerodynamics* 98, 34-46.
- Liu, H., H. Q. Tian and Y. F. Li (2009). Short-term forecasting optimization algorithms for wind speed along Qinghai-Tibet railway based on different intelligent modeling theories. *Journal of Central South University* 16(4), 690-696.
- Liu, Q. K., Y. L. Du and F. G. Qiao (2008). Train-crosswind and Strong Wind Countermeasure Research in Japan. *Journal of the China Railway Society* 30(1), 82-88.
- Liu, T. H. and Zhang J. (2013). Effect of landform on aerodynamic performance of high-speed trains in cutting under cross wind. *Journal of Central South University* 20(3), 830-836.
- Rezvani, M. A. and M. Mohebbi (2014). Numerical calculations of aerodynamic performance for ATM train at crosswind conditions. *Wind and Structures* 18(5), 529-548.
- SNCF I / SYSTRA (2004). Consulting report of CHI High-speed railway on engineering design. *Report, SNCF I / SYSTRA*.
- Suzuki, M., K. Tanemoto and M. Tatsuo (2003). Aerodynamics characteristics of train/vehicles under cross winds. *Journal of Wind Engineering and Industrial Aerodynamics* 91(1), 209-218.
- Wang Y., Y. Xin, Z. h. Gu, S. h. Wang, Y. Deng and X. Yang (2014). Numerical and Experimental Investigations on the Aerodynamic Characteristic of Three Typical Passenger Vehicles. *Journal of Applied Fluid Mechanics* 7(4), 659-671.
- Ye, W. J., H. G. Liu and J. Xue (2001). Monitoring, Forecasting and Early Warning System for Severe Weather along the Railway Line. *Bimonthly of Xinjiang Meteorology* 24(6), 25-27.
- Zhang, J., G. J. Gao and L. J. Li (2013). Height optimization of windbreak wall with holes on high-speed railway bridge. *Journal of Traffic and Transportation Engineering* 13(6), 28-35.
- Zhang, J., X. F. Liang, T. H. Liu and L. F. Lu (2011). Optimization Research on aerodynamic shape of passenger car body with strong crosswind. *Journal of Central South University (Science and Technology)* 42(11), 3578-3584.
- Zhang, J. and T. H. Liu (2012). Optimization Research on the Slope Angle of the Earth Type Windbreak Wall of Xinjiang Single-Track Railway. *China Railway Science* 33(2), 28-32.